Optica Applicata, Vol. LIV, No. 4, 2024
DOI: 10.37190/oa/195576

Phase unwrapping method based on improved U-net network

Jiansu Li, Jingjing Zhang, Changying Dang*, Haowen Chen, Zhao Yang, Junsheng Zhao

North University of China, College of Mechanical Engineering, Taiyuan, 030051, China

*Corresponding author: dangchangying@163.com

In order to solve the problem of unwrapping the phase in digital holographic reconstruction, a new convolutional architecture is proposed. The proposed method takes the U-net network as a framework, and incorporates the lightweight deep learning network of Mobilenetv1 in the encoding part to reduce the model complexity, the number of parameters, and the cost of computation; and proposes a complex dual-channel convolutional block in the decoding part instead of the 3×3 convolution in the original U-net network, which fully incorporates the features in the decoding process. (abbreviated as DC-UMnet network) Meanwhile, the loss value is calculated using the SmoothL1Loss function, and the activation function uses ReLU6. Finally, the simulated dataset containing noise is used for training; and the experimentally obtained wrapped phase maps is used for verifying. The simulation results show that under different degrees of noise conditions, compared with the DCT method and the deep learning phase unwrapping network, the structural similarity index values of the DC-UMnet network are improved by 0.416 and 0.064; and the normalized root-mean-square errors are reduced respectively by 13.2% and 5.8%. Through the actual measurement data, the proposed network model of the feasibility and good noise reduction ability are verified, which can realize digital holographic phase unwrapping in a simple, fast and efficient way.

Keywords: digital holography, deep learning, DC-UMnet network, phase unwrapping.

1. Introduction

Digital holographic microscopy [1] is a combination of digital technology and traditional optical holographic imaging technology, which through the interference between the object light wave and the reference light wave, the phase information is recorded in the form of interference fringes and phase reconstruction is carried out by computer. Digital holographic microscopy, as a non-destructive measurement technology, has the advantages of no marks, no damage and high-precision fast phase imaging [2], and it is widely used in the fields of three-dimensional topographic measurement, industrial inspection, microscopic particle imaging and biomedical interferometry [3-6]. In the digital holographic reconstruction process, the phase wrapped in the $(-\pi, \pi]$ interval obtained by using the inverse tangent function calculation. The difficulty lies in the need to obtain the real phase information through the phase unwrapping operation.

In order to solve this problem, researchers have successively proposed a variety of phase unwrapping methods to achieve complex phase unwrapping. For example, the improved three frequency heterodyne synthesis phase unwrapping method [7], the time series phase unwrapping algorithm based on the L_P norm optimized compressed perception [8], and the weighted least square phase unwrapping algorithm based on the reliability mask [9]. The improved three-frequency heterodyne synthesis phase unwrapping method introduces Otsu segmentation to judge the phase threshold according to the distribution found during phase difference calculation. It improves the measurement accuracy through calculating by phase difference and phase sum. This method can reduce the influence of noise and further improve the accuracy of measurement results, but it cannot guarantee the speed of phase unwrapping. In the case of strong noise and steep gradient, the time series phase unwrapping algorithm based on L_P norm optimization compression perception transforms the minimized L_0 norm problem into a non-convex problem with weak constraints. It is an optimized compressed sensing model which combines the constraint criterion of phase triplet closure in time domain and the solution strategy of iterative reweighted least square method. The weighted least squares unwrapping algorithm based on reliability mask has strong anti-noise ability and robustness. However, for phase maps with more texture characteristics, the phase of the edge of the masked object is smoothly suppressed in the unwrapping operation. The result is a large phase error. To sum up, there are currently two mainstream research directions of phase unwrapping algorithms: the first is to improve the speed of unwrapping, and the second is to improve the quality of unwrapping in the case of strong noise. The traditional phase unwrapping method has now entered into a bottleneck period. And it is expected to use deep learning to improve the speed, quality and robustness of phase unwrapping.

In recent years, deep learning technology has developed rapidly and made some achievements in phase unwrapping technology. At the same time, the paper solves the phase unwrapping problem based on deep learning technology. The U-net [10] network architecture based on deep learning semantic segmentation provides new ideas and methods for phase unwrapping. It can be used for general research on Gaussian functions to process simulated phase data. The results show excellent anti-noise performance and anti-aliasing performance. PhaseGAN [11], a fractal learning method based on generating adversarial networks, is used to solve the problem that the deep learning architecture relies on the paired data set. It is only applicable to the fully corresponding data, while ignoring the physical characteristics of the imaging process. In view of the phase wrapping problem encountered by biological samples in digital holographic microscopy imaging, the Pix2Pix [12] network is used for phase unwrapping operation, and the digital holographic microscopy image of biological cells is used for verification. The computing speed of this network has been greatly improved. Moreover, the depth Fourier channel attention Network (DFCAN) [13] uses the differences of various features in the frequency domain content to learn the high-frequency information of various biological samples. Compared with other methods, this network image has

better enhancement effect, stronger robustness and generalization ability. Fourier domain focusing of DFCAN can achieve robust reconstruction of SIN images under low SNR conditions. In the complex phase field of noise, discontinuity and aliasing, it is necessary to design the network for these problems to improve the robustness and effectiveness of traditional methods. For example, phase unwrapping technology based on U-net network [14] and phase unwrapping technique based on adversarial neural network [15]. The choice of loss function in the method of deep learning phase unwrapping is very important. For example, PhaseNet [16] network architecture classifies phase unwrapping as a semantic segmentation problem. The network adopts a new type of loss function, which is robust to noise. It integrates residuals by minimizing the step difference and takes advantage of L1 losses to overcome the problem of class imbalance. Another example is that the MNet [17] network promotes the fusion of shallow information and deep features through a rich jump connection structure, while using the structural loss function.

For the problem of phase unwrapping under serious noise conditions, an anti-noise phase unwrapping method is needed to accurately and quickly realize phase unwrapping. Based on U-net network, this paper proposes a phase unwrapping method based on DC-UMnet network.

2. The principle of phase unwrapping in DC-UMnet network

The principle of digital holographic phase unwrapping can be explained by the following equation:

$$\varphi(x, y) = \phi(x, y) + 2\pi k \tag{1}$$

where $\varphi(x, y)$ is the wrapped phase, $\phi(x, y)$ is the real phase. The phase unwrapping means that the k value is estimated from the wrapped phase $\varphi(x, y)$, so that the real phase of the object $\phi(x, y)$ is obtained.

Figure 1 shows the process of the DC-UMnet network phase unwrapping method, which is mainly divided into two parts. The network training process is shown in Fig. 1(a) and the network test process is shown in Fig. 1(b). The mapping relationship between the wrapped phase and the real phase is established according to Eq. (1). The orange part in Fig. 1(a) is the data set generation stage, and the blue part is the network training stage. The best model weight of the network is obtained through training. After the training is completed, the wrapped phase map collected by the experiment is entered into the network shown as Fig. 1(b), and the network will automatically call the established mapping relationship for phase unwrapping.

2.1. DC-UMnet network structure

The feasibility of a deep learning network is crucial. Since the U-net network based on the encoding part and the decoding part structure has been widely used to perform

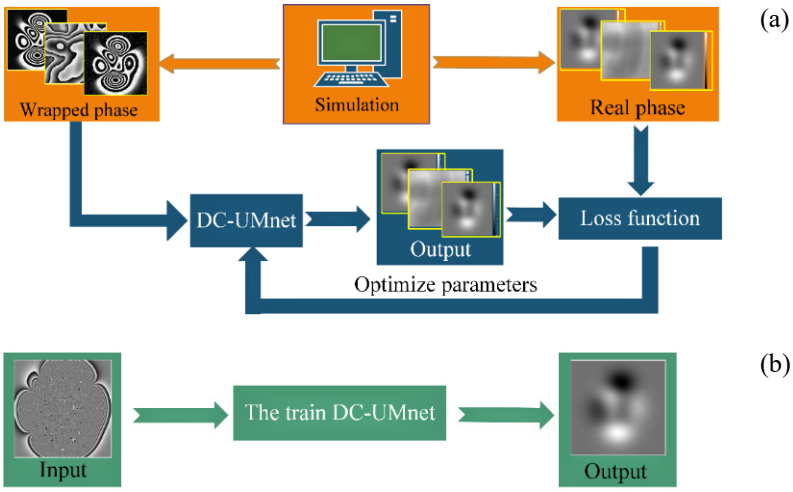

Fig. 1. Phase unwrapping flowchart of the DC-UMnet network. (a) Training process, and (b) testing process.

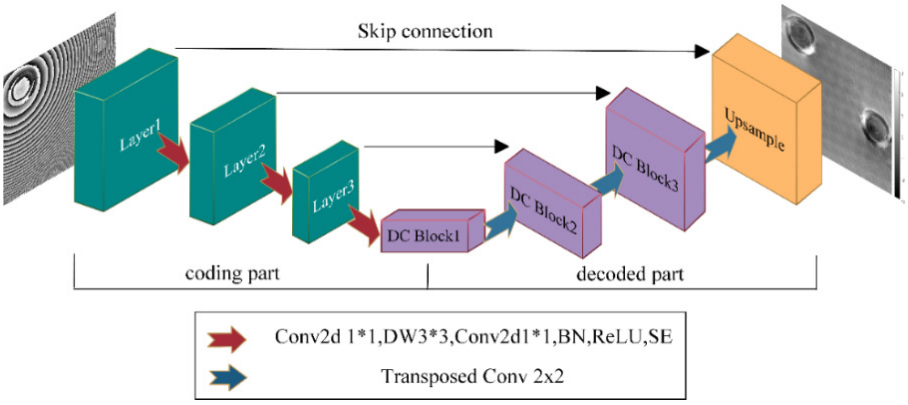

Fig. 2. Network structure of DC-UMnet.

different tasks. Therefore, a DC-UMnet network based on this structure is constructed as shown in Fig. 2. On the basis of the U-net network, the DC-UMnet network integrates the lightweight deep learning network of MobileNetv1 in its coding part, which is conducive to reducing the complexity, number of parameters and computing cost of the model. In order to improve the feature extraction ability and anti-noise ability of the model, a complex dual-channel convolution module (hereinafter referred to as DC Block) replaces the 3×3 convolution in the original U-net network.

Since MobileNetv1 requires little computation and runs fast, the lightweight network of MobileNetv1 is embedded into the U-net network architecture, as shown in Fig. 3 and the number of channels is shown in Table 1. Input represents the number of

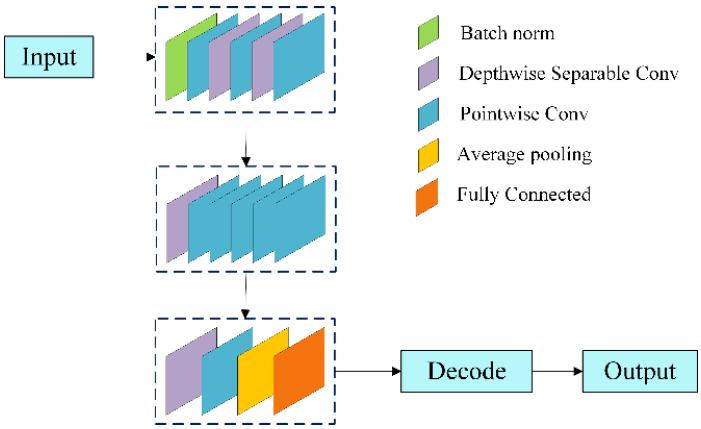

Fig. 3. Left coding part of DC-UMnet.

input channels, Conv_pw represents point-by-point convolution, Conv_dw represents deep convolution, and output represents the number of output channels, stride represents the convolutional stride. Compared with the traditional convolution method, the deep separable convolution greatly reduces the amount of parameters and calculation.

T a b l e 1. Left coding part and bridge path.

Layer	Input	Operator	Output	Stride
1	3	Conv_bn	32	2
1	32	Conv_pw	64	1
1	64	Conv_dw	128	2
1	128	Conv_pw	128	1
1	128	Conv_dw	256	2
1	256	Conv_pw	256	1
2	256	Conv_dw	512	2
2	512	Conv_pw	512	1
2	512	Conv_pw	512	1
2	512	Conv_pw	512	1
2	512	Conv_pw	512	1
2	512	Conv_pw	512	1
3	512	Conv_dw	1024	2
3	1024	Conv_pw	1024	1
3	1024	Avg Pool	1024	1
3	1024	FC	1024	1

The right decoding part in Fig. 2 consists of the DC Block module, also known as the dual-channel convolution module. The DC Block module is symmetrical as a whole, and three 3×3 convolutional layer sequences are used on the left and right sides shown

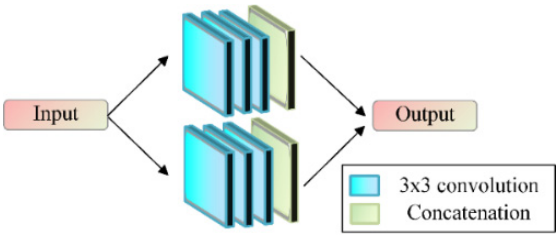

Fig. 4. Decoding part module.

as Fig. 4. It achieves the purpose of fully fusing the characteristic information containing noise, so as to realize the phase unwrapping.

2.2. Activation function and loss function

2.2.1. Activation function

The ReLU6 function has been proved by many deep learning tasks to have the advantages of good gradient propagation effect, sparse activation and high calculation efficiency. Therefore, the DC-UMnet network uses the ReLU6 function to activate the extracted feature diagram nonlinearly. ReLU6 function $f(x)$ can be expressed as:

$$f(x) = \begin{cases} 0, & x \le 0 \\ x, & 0 < x \le 6 \\ 6, & x > 6 \end{cases} \tag{2}$$

where x is the input value.
Compared with activation functions such as Sigmoid and Tanh, the convergence speed of the ReLU6 activation function is much faster. The ReLU6 function $f(x)$ is used to suppress the maximum value, which helps to maintain accuracy when quantifying the mode. It can also reduce the amount of computing on the network to improve the network training speed and increase the nonlinearity of network. Moreover, it reduces overfitting and prevents the gradient from disappearing.

2.2.2. Loss function

The loss function is a reflection of the model's degree of data fitting. In the training of the neural network, the selection of the loss function and the adjustment of various parameters of the gradient decline are particularly important. The smaller the loss function, the better the robustness of the model. The choice of the loss function depends on many factors, including whether there is a group point, the time efficiency of the operating gradient drop, whether it is easy to find the derivative of the function, and the confidence of the predicted results. The paper uses SmoothL1Loss to calculate the loss value, as shown in the following equation:

$$\text{SmoothL1Loss} = \begin{cases} 0.5x^2, & |x| < 1 \\ |x| - 0.5, & x < -1 \quad \text{or} \quad x > 1 \end{cases} \tag{3}$$

In Eq. (3), x is the numerical difference between the predicted value and the real value.

Compared with the loss functions L1 loss and L2 loss commonly used in deep learning, SmoothL1Loss improves the zero-point non-smoothing problem. It has excellent robustness to outliers in the training data, and can control the gradient level to avoid affecting the final training effect of network due to special points.

3. Network training

3.1. Generation of simulation data sets

Assuming that $\varphi(x, y)$ is the true phase and the $\psi(x, y)$ is wrapped phase, the relationship between them is shown in the following equation:

$$\psi(x, y) = \text{angle}\{\exp[i\varphi(x, y)]\} \tag{4}$$

In Eq. (4), i is an imaginary unit, and the angle function uses plural independent variable to wrap the real phase in the $(-\pi, \pi]$ interval.

The phase map randomly generated by MATLAB software is selected as the data set. The initial matrix size is set to a random 2×2 to 8×8, and its value range is set to 10 to 40. Each matrix is expanded to 128×128 by interpolation. The generated two-dimensional phase distribution is used as the real phase. Then, we generate the corresponding wrapped phase according to Eq. (4). The simulated wrapped phase and the corresponding unwrapped phase are calibrated in pairs. And the 30% data set is added noise to improve the anti-noise ability of the network. Before all wrapping phases are wrapped, pepper and salt noise [0, 0.05, 0.10, 0.15, 0.20] is randomly assigned to simulate no noise, light noise, moderate noise and severe noise in real data respectively. A total of 25,000 unwrapped phases are generated, and the corresponding simulated wrapped phase is obtained through Eq. (4). The simulated wrapped phase and the corresponding simulated unwrapped phase are calibrated in pairs, in which 23,500 pairs are used for training and 1,500 pairs are used for testing.

3.2. Network training environment

This experiment is run in PyCharm software. The host uses Intel(R) Core(TM) i5-9300, the CPU running frequency is 2.4 GHz, the graphics card is Nvidia GeForce GTX 1650, and the memory is 11. 8G. This paper uses the PyTorch (Python3.8) deep learning framework in the Anaconda environment for network training. The model parameter learning rate is set to 0.01, the batch size is set to 32, the loss function uses SmoothL1Loss, and the optimizer uses Adam (adaptive moment estimation).

3.3. Effect evaluation indicators of network models

Structural similarity index (SSIM) is used to objectively evaluate the results of simulated test solutions. It can intuitively reflect the human eye's perception of the image.

The SSIM value is within the [–1, 1] range. The closer the value of SSIM is to 1, the more similar the two images and the higher the quality. The farther the SSIM is from 1, the greater the difference between the two images and the lower the quality. The expression of the SSIM is as follows:

$$\mathrm{SSIM}(x, y) = \frac{(2\mu_x\mu_y + C_1)(2\sigma_{xy} + C_2)}{(\mu_{x^2} + \mu_{y^2} + C_1)(\sigma_{x^2} + \sigma_{y^2} + C_2)} \tag{5}$$

where x and y represent the predicted phase and real phase, respectively; μ represents the mean value; σ represents the standard deviation; σ_{xy} is the covariance of x and y; C_1 and C_2 are two constants, which are used to avoid zero in the denominator and to control contrast and structure.

Normalized root mean square error (NRMSE) is an indicator that evaluates the difference between prediction results and real results, and is often used for model evaluation of regression problems. It normalizes the root mean square error (RMSE) to the range of the predicted value, making the comparison between different data sets and problems more fair. The expression of the NRMSE is as follows:

$$\mathrm{NRMSE} = \frac{\sqrt{\mathrm{MSE}}}{y_{\max} - y_{\min}} \tag{6}$$

where MSE is the mean square error; $y_{\max}$ and $y_{\min}$ are the maximum and minimum values of the predicted value and the real value, respectively.

4. Experimental results and analysis

4.1. Simulation test results

The data set generated by the above method is used for simulation for experimental verification. Five wrapped phase maps are randomly selected in the test set for DC-UMnet network training and tested shown as Fig. 5. The unwrapped phase map randomly generated based on MATLAB software is shown in Fig. 5(b), and the corresponding wrapped phase map generated according to Eq. (4) is shown in Fig. 5(a). Figure 5(c) is the unwrapped phase map generated by the DC-UMnet network.

The SSIM index of the DC-UMnet network phase unwrapping results in Fig. 5 is 0.996, 0.998, 0.997, 0.996 and 0.998, respectively. Its normalized mean root error is 0.88%, 0.89%, 0.89%, 0.87% and 0.86%, respectively. The results above indicate that phase unwrapping can be completed well.

4.2. Anti-noise performance test

In the actual measurement, there are various noises in the environment where the phase maps are obtained, so the anti-noise ability of the DC-UMnet network needs to be tested. By unwrapping the phase under different degrees of noise conditions, the anti-noise

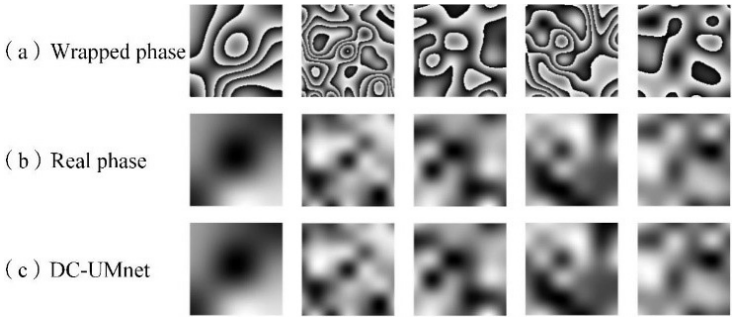

Fig. 5. Simulation test set test results.

ability of the network model is verified. DCT method, U-net network, DC-Unet network, Res-Unet network and DC-UMnet network were used to unwrap the simulated phase containing pepper and salt noise density P of 0.03, 0.06, 0.09, 0.12, 0.15, 0.18 and 0.21, respectively, and the results are shown in Fig. 6. It can be seen that the phase unwrapping results of U-net, DC-Unet and Res-Unet networks have the problem of

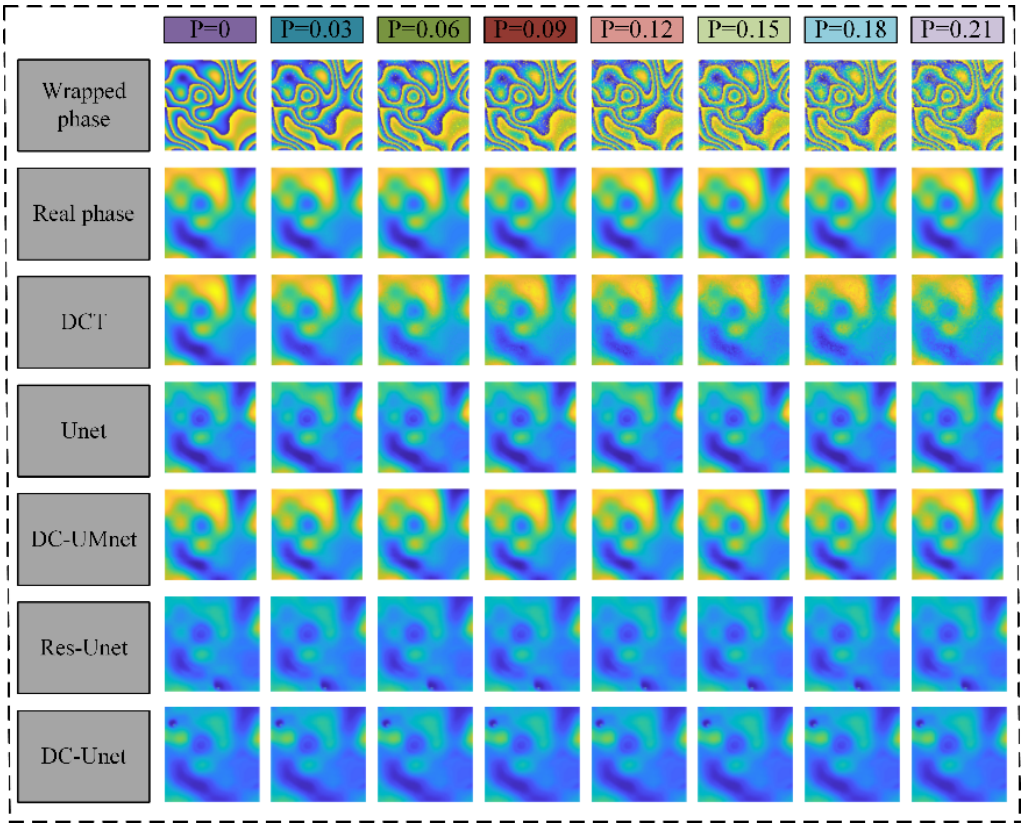

Fig. 6. Results of phase unwrapping.

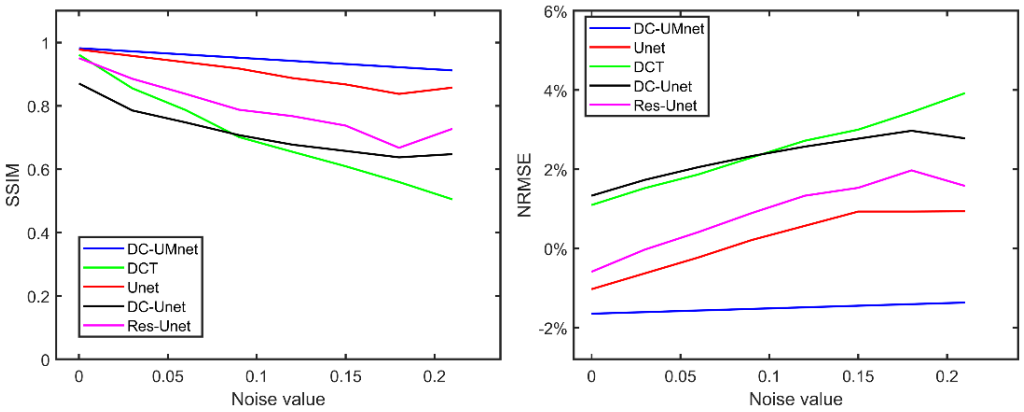

Fig. 7. Performance comparison of different methods.

T a b l e 2. The performance indexes of phase unwrapping results of different methods.

Method	$SSIM_B$	$SSIM_A$	$NRMSE_B$	$NRMSE_A$
Our method	0.990	0.921	0.88%	1.58%
DCT	0.961	0.505	7.74%	14.82%
U-net	0.977	0.857	2.43%	7.35%
DC-Unet	0.871	0.648	8.33%	11.94%
Res-Unet	0.951	0.728	3.53%	8.95%

phase information loss. In addition, with the increase of noise severity, the phase unwrapping results of DCT are gradually unsatisfactory.

The performance comparison of the above five methods is shown in Fig. 7. The performance indexes of phase unwrapping results of different methods are shown in Table 2. $SSIM_B$ indicates the SSIM value before the change and $SSIM_A$ indicates the SSIM value after the change. $NRMSE_B$ indicates the NRMSE value before the change, and $NRMSE_A$ indicates the NRMSE value after the change. Compared with other methods, the SSIM value of the proposed phase unwrapping method is increased by 0.2365 on average, and the normalized mean square error is reduced by 9.18% on average. Experimental results show that this method has good phase expansion ability and anti-noise ability.

4.3. Experimental test results

4.3.1. Record of hologram

In order to verify the feasibility of this method, the off-axis micro holography is used for experimental verification. According to the Mach–Zender optical path, the pre-amplified digital holographic recording optical path schematic diagram is shown in Fig. 8. The laser in the optical path is THORLABS HRS015 helium-neon laser, with a power of 1.2 mW and a wavelength of 632.992 nm. The objective lens is made of OLYMPUS

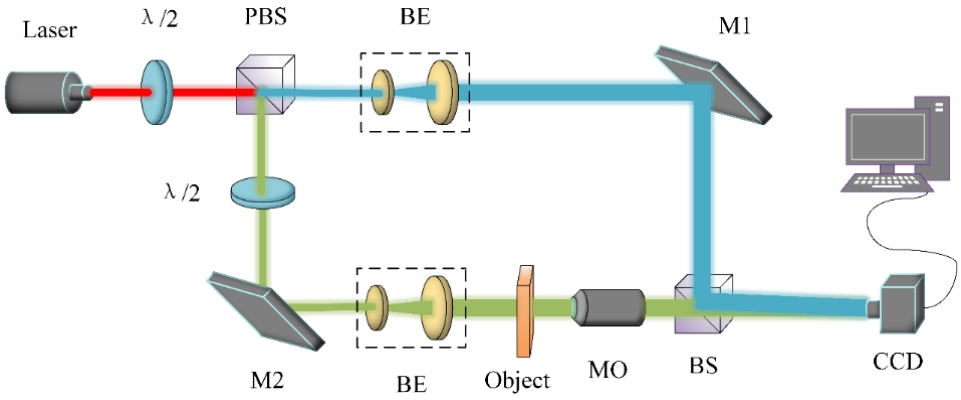

Fig. 8. Optical path diagram of experimental recording.

MPLFLN20X microscopic objective lens, with a magnification of 20 times and a focal length of 9 mm. The camera uses Basler's acA4112-30 μm industrial camera with a resolution ratio of 4096×3000 and a pixel size of 3.45×3.45 μm.

In Fig. 8, the light emitted by the He-Ne laser is divided into two beams through the 1/2 wave sheet and the polarization beam prism PBS. One beam is used as a reference light wave after beam expansion through the alignment beam BE. The other beam passes through the 1/2 wave plate $\lambda/2$ and then passes through the reflector M2 to illuminate the object directly, and is amplified by the microscopic objective lens MO as the object light wave. The object light wave and the reference light wave interfered on the CCD target surface to form a hologram after the beam was combined through the beam splitting prism BS. The beam splitting prism BS is also used for the Angle between the object light and the reference light in off-axis holography to ensure the separation of zero-order and positive and negative first-order spectrum. During the experiment, the neutral filter NF is used with two 1/2 wave pieces to adjust the light intensity of the whole light path.

4.3.2. Analysis of experimental results

The experimental structure adopts a pre-amplified digital holographic optical path, and the principle of the optical path and the experimental platform are shown in Subsection 4.3.1. In order to verify the feasibility of the network, a round-hole and a step were etched on transparent quartz glass. The diameter of the circular hole is 30 μm and the depth of the hole is 312 nm. The step is 70 μm long, 20 μm wide and 360 nm deep. The refractive indices of quartz glass and air are n_s = 1.458 and n_m = 1, respectively. The hologram recorded by the CCD camera is shown in Fig. 9.

The above five methods are used to unwrap the phase of the two samples, respectively. The result of phase unwrapping is shown in Fig. 10. The experimental results show that the phase unwrapping results of DC-UMnet are clear. Due to the influence of background noise, the results of unwrapping by DCT method are not clear. Some phase information is lost in phase unwrapping using Unet, Res-Unet and DC-Unet net-

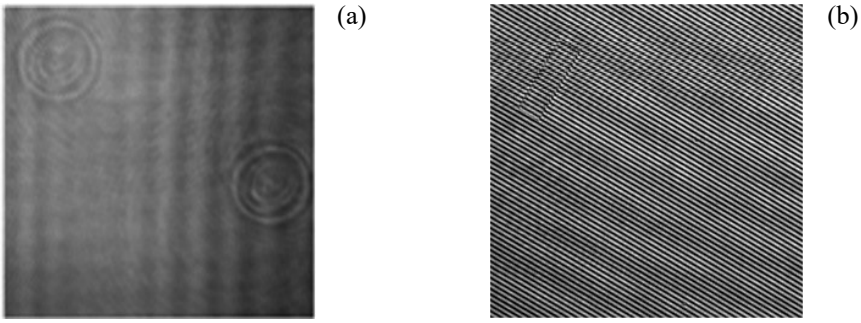

Fig. 9. Sample hologram. (a) Round-hole hologram, and (b) step hologram.

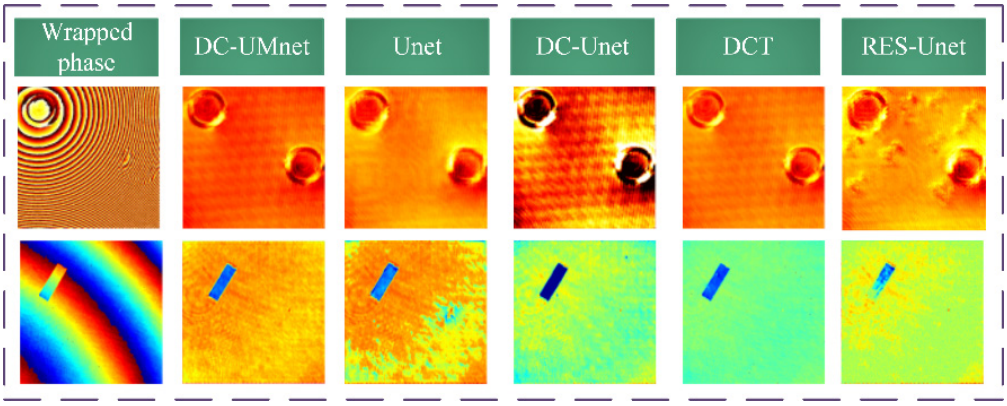

Fig. 10. The results of sample phase unwrapping.

works. There is no phase diagram in the training set which is exactly consistent with the actual measurement, but the proposed method still understands the phase wrapping, which proves the feasibility of the network.

Round-hole sample

In order to further evaluate the effect of various methods of phase unwrapping, the cut-off line shown in Fig. 11(a) is intercepted at the center of the round-hole in the same area of the phase map of Fig. 10, and the interception results are shown in Fig. 11(b). The size of the round-hole is obtained by taking the mean in the interception results of Fig. 11. As shown in Table 3, D and H in the table represent the diameter and depth of the circular hole, respectively, and E_{D} and E_{H} represent the errors of the diameter and depth of the circular hole, respectively.

From the data in Table 3, in the DC-UMnet network phase unwrapping results, the absolute error of the diameter size obtained is smaller than the other four methods. The absolute error of the depth size obtained is about 68.1 nm, which is the smallest error among the five methods. It shows that the DC-UMnet network is feasible.

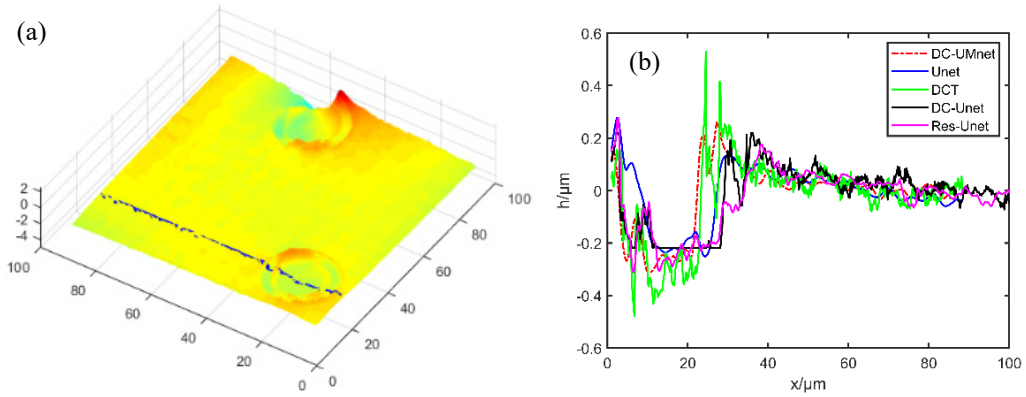

Fig. 11. Circular hole Section contour of reconstructed image. (a) Circular hole intercept position of unwrapping phase. (b) Circular hole intercept result of unwrapping phase.

T a b l e 3. Dimensions and errors of round-hole obtained by unwrapping phase with different methods.

Method	D [μm]	H [μm]	E_D [μm]	E_H [μm]
DC-UMnet	26.52	0.2439	–3.48	–0.0681
U-net	25.92	0.2108	–4.08	–0.1012
DCT	23.92	0.3876	–6.08	0.0756
DC-Unet	33.53	0.1891	3.53	–0.1229
Res-Unet	35.73	0.2185	5.73	–0.0935

Step sample

To further evaluate the generalization of the network, other samples were studied using the network. The lateral dimensions and errors of the steps are obtained according to the step phase diagram in Fig. 12, as shown in Table 4, where L and W respectively

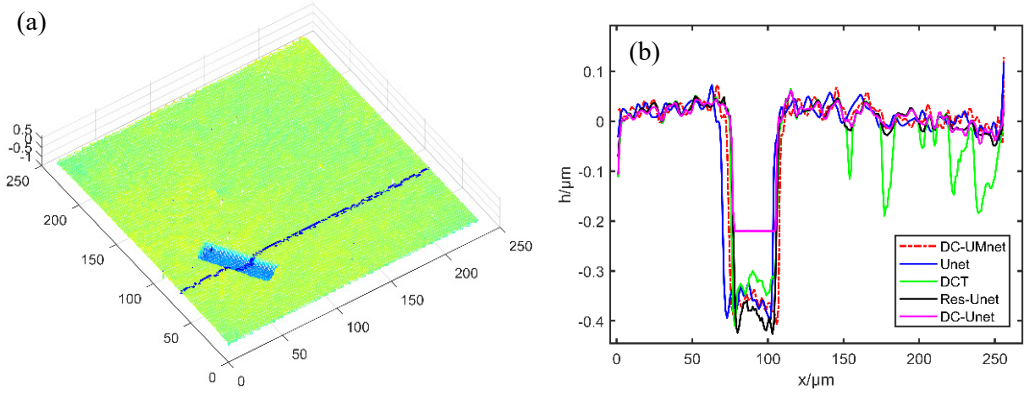

Fig. 12. Step section contour of reconstructed image.(a) Step intercept position of unwrapping phase. (b) Step intercept result of unwrapping phase.

T a b l e 4. Dimensions and errors of step obtained by unwrapping phase with different methods.

Method	L [μm]	W [μm]	E_L [μm]	E_W [μm]
DC-UMnet	19.64	69.51	−0.36	−0.49
U-net	17.31	65.73	−2.69	−4.27
DCT	17.47	62.97	−2.53	−7.03
DC-Unet	16.74	60.97	−3.26	−9.03
Res-Unet	17.47	59.73	−2.53	−10.27

represent the length and width of the steps, and E_L and E_W respectively represent the length and width errors.

As can be seen from Table 4, the absolute error of DCT phase unwrapping method is as high as 7.03 μm and the absolute error of U-net network phase unwrapping method is as high as 4.27 μm. The absolute error of DC-Unet phase unwrapping method is as high as 9.03 μm and the absolute error of Res-Unet network phase unwrapping method is as high as 10.27 μm, while the DC-UMnet network phase unwrapping method has

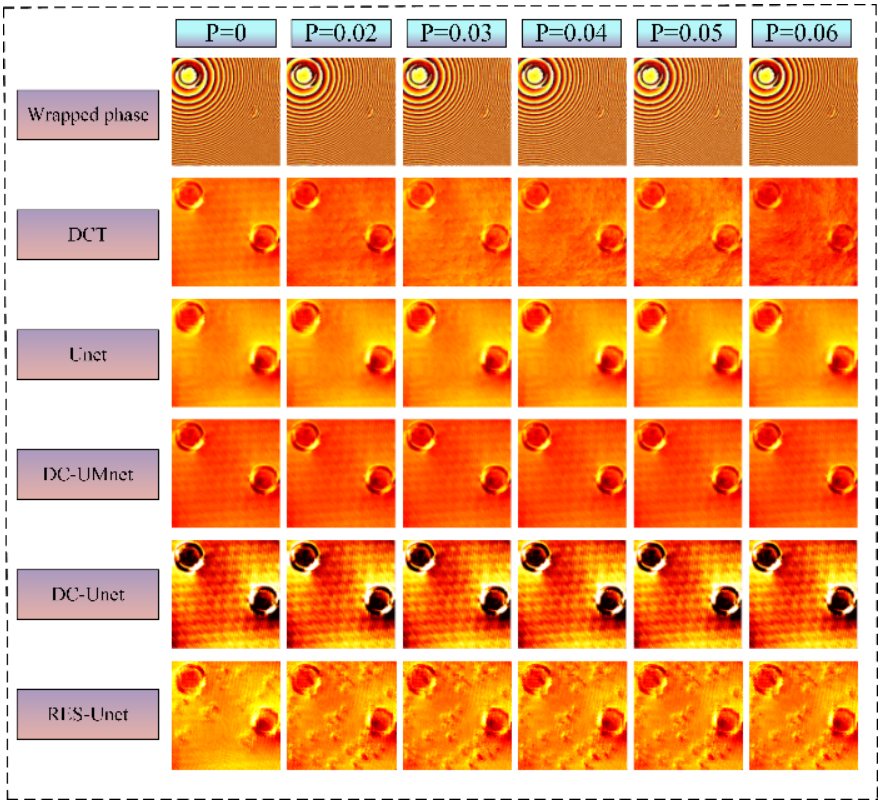

Fig. 13. Phase unwrapping of circular hole after adding noise of different salt and pepper density. Phase unwrapping result of round hole.

considerable accuracy. To further evaluate the above five phase unwrapping methods, a one-dimensional height profile of the reconstructed phase step is given in Fig. 12.

As can be seen from Fig. 12(b), the phase step obtained by DC-Unet network is deformed. The phase step depth obtained by U-Net network is 331.3 nm and the corresponding absolute error is 29 nm. The phase step depth obtained by DC-UMnet network and DCT method is 365.1 and 366.9 nm. The phase step depth obtained by DC-Unet network and Res-Unet network is 219.8 and 388.5 nm. Their corresponding absolute error is 5.1, 6.9,140.2 and 28.5 nm, respectively. The results show that the DC-UMnet phase unwrapping method can improve the measurement accuracy.

The anti-noise ability of the network is tested. The noise with a salt and salt density of 0, 0.02, 0.03, 0.04, 0.05 and 0.06 is added to the sample respectively shown as Figs. 13 and 14. Then, the unwrapping phase is achieved by DCT method, U-net network, DC-UMnet network, Res-Unet network and DC-Unet network. The experimental results show that under salt-and-pepper noise, the background noise of DCT method is obvious while some phase information is missing in U-net, DC-Unet and Res-Unet phase unwrapping results. The phase unwrapping result of the algorithm proposed in this paper is well and less affected by the background noise.

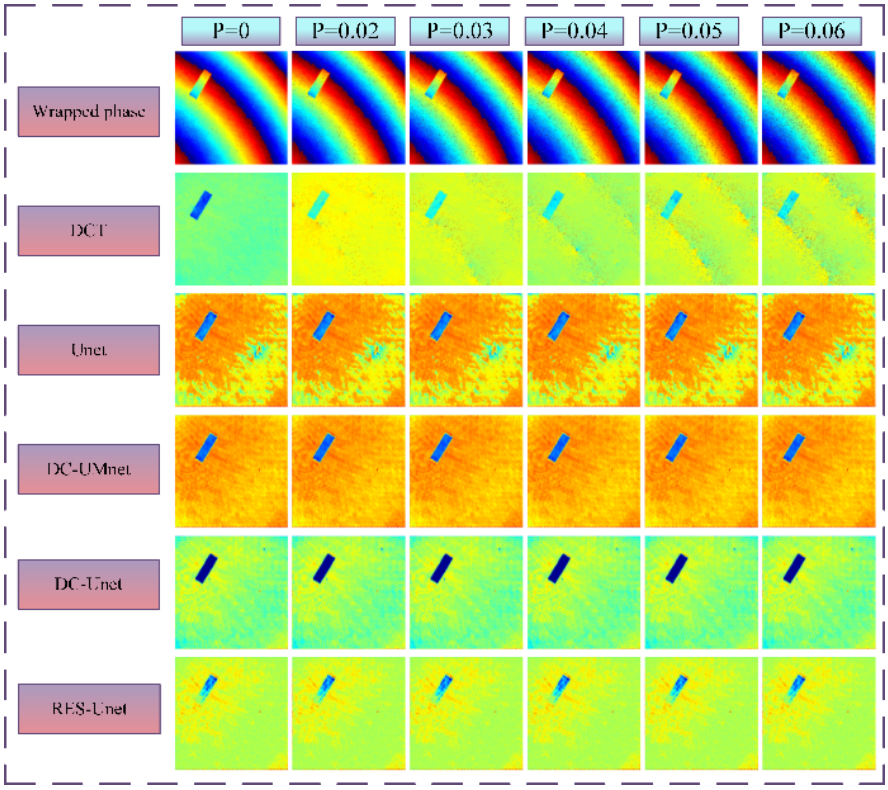

Fig. 14. Phase unwrapping of circular hole after adding noise of different salt and pepper density. Phase unwrapping result of step.

5. Conclusion

In order to achieve high-precision digital holographic phase unwrapping, the paper proposes a phase unwrapping method based on DC-UMnet network. The proposed method uses simulation data for network training and experimental data for network verification. The simulation results show that comparing the proposed method with the other methods, the SSIM value of the proposed phase unwrapping method is increased by 0.2365 on average, and the normalized mean square error is reduced by 9.18% on average. The experimental results show that the transverse dimension error and longitudinal dimension error of the proposed method for the round-hole sample are approximately 3.5 μm and 68.1 nm, respectively. Compared with the other four methods, the transverse dimension error of the proposed method is reduced by 1.38 μm on average, and the longitudinal dimension error is reduced by 30.2 nm on average. The experimental results show that the absolute error of DCT phase unrolling method is up to 7.03 μm, and the absolute error of U-net, DC-Unet and Res-Unet phase unrolling method is up to 4.27, 9.03, and 10.27 μm, respectively. The DC-UMnet network phase unwrapping method has quite high precision. The results show that the phase unwrapping method in this paper has good noise reduction ability, and can realize digital holographic phase unwrapping in a simple, fast and efficient way.

Acknowledgements
This work was supported by the Fundamental Research Program of Shanxi Province (20210302123047, 202103021224199).

References

[1] NGUYEN T.L., PRADEEP S., JUDSON-TORRES R.L., REED J., TEITELL M.A., ZANGLE T.A., *Quantitative phase imaging: Recent advances and expanding potential in biomedicine*, ACS Nano **16**(8), 2022: 11516-11544. https://doi.org/10.1021/acsnano.1c11507

[2] KEMPER B., ILLY E., *Digital holographic microscopy*, Photonics Views **17**(1), 2020: 32-35. https://doi.org/10.1002/phvs.202000007

[3] BAI C., PENG T., MIN J.W., LI R., ZHOU Y., YAO B., *Dual-wavelength in-line digital holography with untrained deep neural networks*, Photonics Research **9**(12), 2021: 2501-2510. https://doi.org/10.1364/PRJ.441054

[4] DE GROOT P.J., DECK L.L., SU R., OSTEN W., *Contributions of holography to the advancement of interferometric measurements of surface topography*, Light: Advanced Manufacturing **3**(2), 2022: 258-277. https://doi.org/10.37188/lam.2022.007

[5] GAO Y.Z., WANG J., TANG J.B., LIU J.J., YAN Q., HUA D.X., *Dispersion of cloud droplet based on pulsed digital holographic interferometry*, Acta Optica Sinica **42**(6), 2022: 0609001. https://doi.org/10.3788/AOS202242.0609001

[6] LIU Y.K., XIAO W., CHE L.P., *et al*., *Study on cavitation imaging of cancer cells based on digital holographic microscopy*, Chinese Journal of Lasers **49**(20), 2022: 2007209.

[7] LIU J., TIAN P., LI H., WEI H., DENG G., ZHOU S., MA Z., WANG W., HE L., *An improved synthesis phase unwrapping method based on three-frequency heterodyne*, Sensors **22**(23), 2022: 9388. https://doi.org/10.3390/s22239388

[8] Li S.J., Zhang S.B., Gao Y.D., Li T., Han J.Z., Chen Q., Zhang Y.S., Tian Y., *Time series phase unwrapping algorithm using L^P-norm optimization compressive sensing*, International Journal of Applied Earth Observation and Geoinformation **117**, 2023: 103182. https://doi.org/10.1016/j.jag.2023.103182

[9] Yan L., Zhang H., Zhang R., Xie X., Chen B., *A robust phase unwrapping algorithm based on reliability mask and weighted minimum least-squares method*, Optics and Lasers in Engineering **112**, 2019: 39-45. https://doi.org/10.1016/j.optlaseng.2018.08.024

[10] Wang K., Li Y., Kemao Q., Di J., Zhao J., *One-step robust deep learning phase unwrapping*, Optics Express **27**(10), 2019: 15100- 15115. https://doi.org/10.1364/OE.27.015100

[11] Zhang Y., Noack M.A., Vagovic P., Fezzaa K., Garcia-Moreno F., Ritschel T., Villanueva -Perez P., *PhaseGAN: A deep-learning phase-retrieval approach for unpaired datasets*, Optics Express **29**(13), 2021: 19593-19604. https://doi.org/10.1364/OE.423222

[12] Park S., Kim Y., Moon I., *Automated phase unwrapping in digital holography with deep learning*, Biomedical Optics Express **12**(11), 2021: 7064-7081. https://doi.org/10.1364/BOE.440338

[13] Qiao C., Li D., Guo Y., Liu C., Jiang T., Dai Q., Li D., *Evaluation and development of deep neural networks for image super-resolution in optical microscopy*, Nature Methods **18**(2), 2021: 194-202. https://doi.org/10.1038/s41592-020-01048-5

[14] Xu R.S., Luo X.N., Shen Y.Q., Guo C.W., Zhang W.T., Guan Y.Q., Fu Y.X., Lei L.H., *Research on phase unwrapping technology based on improved U-Net network*, Infrared and Laser Engineering **53**(02), 2024: 20230564. https://doi.org/10.3788/IRLA20230564

[15] Zhou L., Yu H., Pascazio V., Xing M., *PU-GAN: A one-step 2D InSAR phase unwrapping based on conditional generative adversarial network*, IEEE Transactions on Geoscience and Remote Sensing **60**, 2022: 1-10. https://doi.org/10.1109/TGRS.2022.3145342

[16] Spoorthi G.E., Gorthi R.K.S.S., Gorthi S., *PhaseNet 2.0: Phase unwrapping of noisy data based on deep learning approach*, IEEE Transactions on Image Processing **29**, 2020: 4862-4872. https://doi.org/10.1109/TIP.2020.2977213

[17] Xu M., Tang C., Shen Y., Hong N., Lei Z., *PU-M-Net for phase unwrapping with speckle reduction and structure protection in ESPI*, Optics and Lasers in Engineering **151**, 2022: 106824. https://doi.org/10.1016/j.optlaseng.2021.106824

Received August 1, 2024
in revised form November 4, 2024